Journal of Visualized Experiments

In Vivo Quantification of Hip Arthrokinematics During Dynamic Weight-bearing Activities Using Dual Fluoroscopy

--Manuscript Draft--

Article Type:	Invited Methods Collection - JoVE Produced Video
Manuscript Number:	JoVE62792R1
Full Title:	In Vivo Quantification of Hip Arthrokinematics During Dynamic Weight-bearing Activities Using Dual Fluoroscopy
Corresponding Author:	Andrew E. Anderson University of Utah Salt Lake City, Utah UNITED STATES
Corresponding Author's Institution:	University of Utah
Corresponding Author E-Mail:	aea4@utah.edu
Order of Authors:	Penny Atkins
	Niccolo Fiorentino
	Andrew E. Anderson
Additional Information:	
Question	**Response**
Please specify the section of the submitted manuscript.	Medicine
Please indicate whether this article will be Standard Access or Open Access.	Standard Access ($1400)
Please indicate the **city, state/province, and country** where this article will be **filmed**. Please do not use abbreviations.	Salt Lake City, Utah. United States
Please confirm that you have read and agree to the terms and conditions of the author license agreement that applies below:	I agree to the Author License Agreement
Please provide any comments to the journal here.	

TITLE:

In Vivo Quantification of Hip Arthrokinematics During Dynamic Weight-bearing Activities Using Dual Fluoroscopy

AUTHORS AND AFFILIATIONS:

Penny R. Atkins[1,2], Niccolo M. Fiorentino[1,3], Andrew E. Anderson[1,2,4,5]

[1]Department of Orthopaedics, University of Utah, UT 84112, USA
[2]Scientific Computing and Imaging Institute, University of Utah, UT 84112, USA
[3]Department of Mechanical Engineering, University of Vermont, VT05405, USA
[4]Department of Biomedical Engineering, University of Utah, UT 84112, USA
[5]Department of Physical Therapy, University of Utah, UT 84112, USA
*Corresponding Author

Email addresses of co-authors:

Penny R. Atkins (penny.atkins@utah.edu)
Niccolo M. Fiorentino (niccolo.fiorentino@uvm.edu)

Corresponding author:

Andrew E. Anderson (aea4@utah.edu)

KEYWORDS:

Dual fluoroscopy, biplane videoradiography, kinematics, arthrokinematics, hip, markerless tracking

SUMMARY:

Dual fluoroscopy accurately captures *in vivo* dynamic motion of human joints, which can be visualized relative to reconstructed anatomy (e.g., arthrokinematics). Herein, a detailed protocol to quantify hip arthrokinematics during weight-bearing activities of daily living is presented, including the integration of dual fluoroscopy with traditional skin marker motion capture.

ABSTRACT:

Several hip pathologies have been attributed to abnormal morphology with an underlying assumption of aberrant biomechanics. However, structure-function relationships at the joint level remain challenging to quantify due to difficulties in accurately measuring dynamic joint motion. The soft tissue artifact errors inherent in optical skin marker motion capture are exacerbated by the depth of the hip joint within the body and the large mass of soft tissue surrounding the joint. Thus, the complex relationship between bone shape and hip joint kinematics is more difficult to study accurately than in other joints. Herein, a protocol incorporating computed tomography (CT) arthrography, three-dimensional (3D) reconstruction of volumetric images, dual fluoroscopy, and optical motion capture to accurately measure the dynamic motion of the hip joint is presented. The technical and clinical studies that have applied dual fluoroscopy to study form-function relationships of the hip using this protocol are

summarized, and the specific steps and future considerations for data acquisition, processing, and analysis are described.

INTRODUCTION:

The number of total hip arthroplasty (THA) procedures performed on adults aged 45–64 years suffering from hip osteoarthritis (OA) more than doubled between 2000 and 2010[1]. Based on the increases in THA procedures from 2000 to 2014, a recent study predicted that the overall number of yearly procedures may triple over the next twenty years[2]. These large increases in THA procedures are alarming considering that current treatment costs exceed $18 billion annually in the United States alone[3].

Developmental dysplasia of the hip (DDH) and femoroacetabular impingement syndrome (FAIS), which describe an under- or over-constrained hip, respectively, are believed to be the primary etiology of hip OA[4]. The high prevalence of these structural hip deformities in individuals undergoing THA was initially described more than three decades ago[5]. Still, the relationship between abnormal hip anatomy and osteoarthritis is not well understood. One challenge to improving the working understanding of the role of deformities in the development of hip OA is that abnormal hip morphology is very common amongst asymptomatic adults. Notably, studies have observed morphology associated with cam-type FAIS in approximately 35% of the general population[6], 83% of senior athletes[7], and more than 95% of collegiate male athletes[8]. In another study of female collegiate athletes, 60% of participants had radiographic evidence of cam FAIS, and 30% had evidence of DDH[9].

Studies demonstrating a high prevalence of deformities amongst individuals without hip pain point to the possibility that morphology commonly associated with FAIS and DDH may be a natural variant that only becomes symptomatic under certain conditions. However, the interaction between hip anatomy and hip biomechanics is not well understood. Notably, there are known difficulties with measuring hip joint motion using traditional optical motion capture technology. First, the joint is relatively deep within the body, such that the location of the hip joint center is difficult to both identify and track dynamically using optical skin marker motion capture, with errors on the same order of magnitude as the radius of the femoral head[10,11]. Second, the hip joint is surrounded by large soft tissue bulk, including subcutaneous fat and muscle, that moves relative to the underlying bone, resulting in soft tissue artifact[12–14]. Finally, using optical tracking of skin markers, kinematics are evaluated relative to generalized anatomy and thus do not provide insight into how subtle morphological differences might affect the biomechanics of the joint.

To address the lack of accurate kinematics in combination with subject-specific bone morphology, both single and dual fluoroscopy systems have been developed for analyzing other natural joint systems[15–17]. However, this technology has only recently been applied to the native hip joint, likely due to the difficulty in acquiring high-quality images through the soft tissue surrounding the hip. The methodology to accurately measure *in vivo* hip joint motion and display this motion relative to subject-specific bone anatomy is described herein. The resulting

arthrokinematics provide unparalleled ability to investigate the subtle interplay between bone morphology and biomechanics.

Herein, the procedures for acquiring and processing dual fluoroscopy images of the hip during activities of daily living have been described. Owing to the desire to capture whole-body kinematics with optical marker tracking simultaneously with dual fluoroscopy images, the data collection protocol requires coordination between several sources of data. Calibration of the dual fluoroscopy system utilizes plexiglass structures implanted with metallic beads that can be directly identified and tracked as markers. In contrast, dynamic bone motion is tracked using markerless tracking, which utilizes only the CT-based radiographic density of the bones to define orientation. Dynamic motion is then tracked simultaneously using dual fluoroscopy and motion capture data that are spatially and temporally synced.

The systems are synced spatially during calibration through concurrent imaging of a cube with both reflective markers and implanted metal beads and the generation of a common coordinate system. The systems are synced temporally for each activity or capture through the use of a split electronic trigger, which sends a signal to end the recording of the dual fluoroscopy cameras and interrupts a constant 5 V input to the motion capture system. This coordinated protocol enables the quantification of the position of body segments that fall outside the combined field of view of the dual fluoroscopy system, expression of kinematic results relative to gait-normalized events, and characterization of the soft tissue deformation around the femur and pelvis.

PROTOCOL:

Procedures outlined in this protocol were approved by the University of Utah Institutional Review Board.

1. CT arthrogram imaging

1.1. Arthrogram[18]

1.1.1. Schedule a trained musculoskeletal radiologist to perform the arthrogram directly prior to the scheduled CT imaging.

1.1.2. Position the participant on the table with the hip of interest in the field of view of a clinical fluoroscope. Place sandbags on either side of the ankle to prevent rotation of the leg and hip.

1.1.3. Prepare the skin to create a sterile environment. Mark the location where the needle will be inserted (femoral head-neck junction) and anesthetize the soft tissue at the injection site with **2–5 mL** of 1% lidocaine.

1.1.4. Prepare a solution of **20 mL** of 1% lidocaine, **10 mL** of iohexol injection, and **0.1 mL** of 1 mg/mL (1:1000) epinephrine in a 30 mL luer lock syringe.

1.1.5. Two to five minutes after the lidocaine injection, insert a spinal needle just until it contacts the femoral neck; verify the location of the needle by fluoroscopy. Inject a small amount of the prepared solution (<5 mL) and ensure that the injected fluid is contained within the joint capsule with an image from fluoroscopy.

1.1.6. Inject 20–30 mL of the contrast mixture. If additional resistance to the injection is observed, have a study team member manually apply traction to the hip by pulling on the participant's ankle while the participant resists by pulling on the headboard of the table. Inject the remaining contrast mixture, as appropriate.

1.1.7. Verify by fluoroscopy that the contrast agent fills the joint space and covers the femoral head when traction is applied.

1.1.8. Transfer the patient to the CT scanner in a wheelchair or bed to minimize the loss of contrast within the joint capsule.

1.2. Traction and CT imaging

1.2.1. Help the participant into a supine position on the CT gantry.

1.2.2. Place the hare traction splint device under the leg of interest, ensuring that the proximal padded bar rests just distal to the ischium. Attach the hook and loop straps around the thigh and ankle of the participant and apply light traction.

1.2.3. Acquire a scout image and set the field of view to include the entire pelvis and proximal femurs to just below the lesser trochanter for the hips. Set a separate field of view to include the distal femurs and proximal tibias for the knees.

1.2.4. Apply additional traction (have one member of the research team pull on the ankle while another tightens the strap of the hare traction splint) to ensure separation of the joint space. Acquire images **at 120 kVp, 1.0 mm slice thickness, 200–400 mAs** for the hip and **120 kVp, 3.0 mm slice thickness, and 150 mAs** for the knees. Use CARE Dose, an automated exposure control that modulates tube current according to image quality, to minimize the radiation burden to the participant.

1.2.5. Release and remove the hare traction splint device. Assist the participant to a standing position and ensure they feel comfortable putting weight and being mobile on the limb before allowing them to leave.

2. Dual fluoroscopy imaging

2.1. System setup

2.1.1. Apply anthropometrics[19] to estimate the height of the hip joint based on the participant's reported height and use this measurement to estimate the desired height of the center of the field of view of the system.

2.1.2. Position the image intensifiers **approximately 50°** from one another on the side of the instrumented treadmill corresponding to the hip of interest (**Figure 1**).

2.1.3. Position the X-ray emitters to be pointed towards the image intensifiers. Ensure that the distance between the emitter source and the face of the image intensifiers is approximately **100–110 cm**.

NOTE: The recommended distance between the emitter source and the face of the image intensifiers will vary based on system specification and the collimator in the X-ray emitter.

2.1.4. Connect the center of the face of the image intensifier and the corresponding X-ray emitter of each fluoroscope pair using strings or measuring tapes. Verify that the strings (or tapes) cross at the desired location (i.e., in the expected location of the hip joint).

2.1.5. Affix the plate with three lasers to the emitter and the mirror to the image intensifier. Turn on the lasers and refine the alignment of each emitter and image intensifier based on the reflection of the lasers back to the laser source.

2.2. Calibration images

2.2.1. Prepare for the use of radiation by donning lead and placing signage on the entrances to the room. Minimize exposure by having staff wear protection that includes a leaded vest, skirt, gloves, and glasses. Turn on the fluoroscopes and allow the systems to warm up, as necessary.

2.2.2. For all calibration images, set the fluoroscopes to **64 kVp** and **1.4–1.6 mA**, or as otherwise desired.

2.2.3. Open the camera control software on the computer and select the appropriate cameras as **slave** and **master**. Use **external syncing** to the master camera from the slave camera to sync the two cameras.

NOTE: For all recorded activities, save the same frames from both dual fluoroscopy cameras; frames are identified with a number representing the number of frames prior to the electronic trigger signal.

2.2.4. Verify the alignment of the system by affixing a circular metal washer to the center of the image intensifier and attaching the crosshair fixture to the emitter.

NOTE: Once alignment is verified, it is important to avoid contacting the system.

2.2.5. Attach the plexiglass grid to one of the image intensifiers using screws; minimize the force applied in this process to avoid altering the alignment. Acquire fluoroscopy images and save **100 image frames** from each dual fluoroscopy camera of the **grid**. Remove the grid, and repeat the process for the other image intensifier.

2.2.6. Place the 3D calibration cube within the combined field of view of the two fluoroscopes. To do this, place the cube on a stool or platform that is radio-translucent and visually verify that most or all of the cube is within the field of view. Orient the cube such that the calibration beads do not overlap for either dual fluoroscopy camera view. Acquire images and save **100 image frames** of the **cube**.

2.2.7. Before moving the cube, measure and record the approximate location of the cube's origin from each emitter using the coordinate system of the cube. Remove the cube and any associated platform.

2.2.8. Measure and record the distance between the emitter source and the face of the image intensifier for each fluoroscope.

2.2.9. Attach the beaded plexiglass to a long rod or ruler with a rubber band and move it randomly to provide movements ranging the entire field of view of the system. Ensure that the research staff is mindful of the path of radiation and wear protection to minimize exposure (see step 2.2.1). Save **100 image frames** of the **motion**.

2.2.10. Reset the imaging clock used to track exposure time.

2.3. Static trial and adjustment of parameters

2.3.1. Measure the height of the greater trochanter to ensure that the system height is appropriate for the participant.

2.3.1.1. Palpate the thigh to find the bony prominence of the greater trochanter and locate the most superior point, as is possible.

2.3.1.2. As the superior greater trochanter is approximately at the same height as the hip joint, measure the height from the floor to this point and compare it to the height estimation used to set up the dual fluoroscopy system.

2.3.1.3. If necessary, adjust the system height and recalibrate while the participant is being prepped for data capture.

2.3.2. Familiarize the participant with the fluoroscopy system and inform them that they must notify the research team if they come into contact with any of the equipment during the imaging session, as contact with the system negatively affects the accuracy of their data.

2.3.3. Have the participant step onto the treadmill and stand within the field of view of the dual fluoroscopy system. Check participant alignment from the perspective of each emitter and take note of this position from the perspective of where each member of the research team will be standing or sitting during imaging.

2.3.4. Estimate the imaging parameters (kVp and mAs of each emitter and the exposure of the dual fluoroscopy cameras) based on the body mass index (BMI) of the participant and set each fluoroscope accordingly.

NOTE: For the referenced cohort, fluoroscopy settings ranged from **78 to 104 kVp** and **1.9–3.2 mA** with camera exposures of **4.5–7.0 ms**.

2.3.5. Acquire images of the participant during standing and assess the images for contrast.

NOTE: Increased kVp is associated with increased X-ray scatter (increases noise and reduces contrast), lower image resolution, and lower contrast.

2.3.6. Adjust the parameters and repeat image acquisition, as necessary.

2.3.7. Save **100 frames** of the final images to use as a **static** trial.

2.4. Dynamic trials (**Figure 2**)

2.4.1. Prior to the start of the dual fluoroscopy imaging, have the participant walk a known distance while being timed. Use this to determine the self-selected walking speed for both level and incline walking on the treadmill.

2.4.2. Have the participant don a leaded thyroid collar to protect the thyroid.

2.4.3. During dynamic acquisitions, have the researcher, manning the dual fluoroscopy camera control at the dual fluoroscopy workstation, step behind the lead shield, and watch the participant through the viewing window of the shield (**Figure 3**).

2.4.4. For the performance of all walking trials:

2.4.4.1. Inform the participant prior to starting the belt of the treadmill. Ramp the speed of the treadmill up to the appropriate walking speed and let the participant's gait normalize prior to collecting images.

2.4.4.2. For each walking activity, acquire and save at least two full gait cycles.

2.4.4.3. For the inclined walking activity, have the participant step off the treadmill. Unlock the treadmill, set the incline to **5°**, and relock the treadmill before having the participant step back onto the treadmill to perform the activity.

2.4.4.4. Repeat the imaging, such that the activity is recorded twice.

2.4.4.5. Repeat the same process (step 2.4.4.3) to lower the treadmill upon completion of the activity.

2.4.5. For the pivot activities:

2.4.5.1. Have the participant rotate their body position and feet approximately 45° from the front of the treadmill opposite of the direction of the pivot. If desired, ensure that each foot is placed entirely on a single belt of the dual-belt treadmill to allow straightforward processing of the force plate data.

2.4.5.2. Have the participant perform several pivots to and from their end range of motion while watching for the alignment of the pelvis at the end range of motion. Ensure that the motion is performed smoothly as the pivot does not require acceleration to achieve the final position.

2.4.5.3. Based on the position of the pelvis at the end range of motion, have the participant rotate and/or translate their feet such that the pelvis is facing forward on the treadmill and the hip of interest is in the middle of the combined field of view of the fluoroscopes at the end of the pivot.

2.4.5.4. Once the position is optimized, have the participant perform the pivot during dual fluoroscopy imaging and save all frames where the femur and pelvis are visible in both dual fluoroscopy camera views (approximately 200–400 frames) centered about the end range of motion, capturing as much of the pivot as possible.

2.4.5.5. Repeat the imaging, such that the activity is recorded twice.

2.4.6. For the abduction-adduction activity:

2.4.6.1. Have the participant stand in the field of view of the fluoroscopes and raise the leg of interest to approximately 45° out to their side. Remind the participant to avoid torso motion and reduce the range of motion if necessary.

2.4.6.2. Acquire and save all frames where the femur and pelvis are visible in both dual fluoroscopy camera views (approximately 200–400 frames).

2.4.6.3. Repeat the imaging, such that the activity is recorded twice.

2.4.7. For the dynamic hip joint center or star-arc activity[20]:

2.4.7.1. Have the participant stand in the field of view of the dual fluoroscopy system and raise and lower their leg anteriorly and at 45° increments of 180°, ending with a posterior raise

and lower of their leg. Prior to placing their leg back down onto the ground, have the participant circumduct their leg and return to a standing position.

2.4.7.2. Once the participant is comfortable with the motion and can complete it in approximately 6–8 s, acquire and save images of the activity.

NOTE: Only one activity is captured with dual fluoroscopy due to the length of the trial.

2.5. Additional calibration images

2.5.1. If at any point during the data collection, the participant believes they may have come into contact with any part of the fluoroscopic equipment, image the grids and cube and save all the files for calibration.

2.5.2. Upon completion of the data collection, image the grids and cube and save all files for calibration to serve as a backup if any issues arise with the initial calibration.

3. Skin marker motion capture and instrumented treadmill

3.1. System setup

3.1.1. Focus the optical motion capture system on the treadmill (**Figure 3**). Due to the potential issues with visualizing the participant while in the field of view of the dual fluoroscopy system, be prepared to precisely position the infrared cameras to ensure accurate visualization (**Figure 2**).

3.1.2. Turn on the system and use a set of markers to ensure that the dual fluoroscopy system does not prevent visualization of the desired field of view.

3.1.3. Check that the markers are clear and circular and adjust the focus of the infrared cameras, as necessary.

3.1.4. Ensure that the fluoroscopes are covered to reduce any reflective surfaces. Review each infrared camera and **mask** the camera view if the reflective objects cannot be covered.

3.1.5. Set up the motion capture software to read in an external 5 V signal from the electronic trigger used to end camera acquisition of the dual fluoroscopy system. Use this trigger to temporally sync the data from the two systems.

3.2. Calibration

3.2.1. Once the system is on and ready, use the active calibration wand to simultaneously calibrate the optical and infrared motion capture cameras. Ensure that the entire region within

the dual fluoroscopy system is thoroughly captured during the calibration while avoiding contact with any equipment.

NOTE: Wand motions resembling tossing food in a frying pan have worked well.

3.2.2. Due to the obstructions caused by the dual fluoroscopy system, perform the calibration so that all the infrared cameras have **image errors less than 0.2**.

NOTE: The image error for the video camera will be higher, although still less than 0.5. The video camera is not specifically used for any quantification of motion, only for visual recording of the motion capture.

3.2.3. During the acquisition of the cube trial for dual fluoroscopy, also capture the cube with the motion capture infrared cameras. Ensure that the cube has reflective markers affixed to it for the position to be imaged with cameras from both the motion capture and dual fluoroscopy systems.

3.3. Marker set and placement

3.3.1. Before the arrival of the participant, cut and apply double-sided tape (toupee tape) to the base of 21 spherical reflective skin markers. To ensure the longevity of the markers, ensure that the tape or any skin does not come in contact with the reflective markers.

3.3.2. For each of the five marker plates (two on the shank, two on the thigh, one on the back; **Figure 4**), apply spray glue to the skin side of the fabric strap and wrap it tightly around the participant. Check with the participant that the straps feel tight (but are not uncomfortable). Clean hands of any excess spray glue before adhering the rest of the marker set.

3.3.3. Apply five markers to the clavicle, medial knees, and medial malleoli, which are only used for calibration.

3.3.4. Apply the remaining 16 markers to the superior iliac spines (ASIS), posterior superior iliac spines (PSIS), greater trochanter of the femur being imaged, shoulders, sternum, lateral knees, lateral malleoli, and feet (**Figure 4**).

3.3.5. Ask the participant to inform the study team if any markers or straps become loose during the data capture.

3.4. Static trial

3.4.1. In conjunction with the static standing trial from dual fluoroscopy, capture a standing trial for motion capture.

3.4.2. Label all markers. If any markers are not visible by at least three infrared cameras during the acquired static activity, reacquire a static image to ensure that all markers are visible.

3.4.3. Remove the calibration-only markers and have the participant don a thyroid collar to provide radiation protection during the remainder of the data collection.

3.5. Dynamic trials

3.5.1. For each of the dynamic trials captured with the dual fluoroscopy system, acquire motion capture video, ensuring that the entirety of each dual fluoroscopy video is within the bounds of the motion capture acquisition.

3.5.2. Ensure that the break in the 5 V signal from the electronic trigger of the dual fluoroscopy system is captured within each trial.

4. Image preprocessing

4.1. CT-based model

4.1.1. Segment the proximal and distal femur of the side of interest and the entire pelvis, as these bones are used for tracking and/or coordinate system generation.

4.1.2. Ensure that the segmentations are representative of the bone shape in all three imaging planes and appear relatively smooth.

NOTE: The ability to analyze arthrokinematics is dependent on obtaining high-quality reconstructions through careful segmentation.

4.1.3. Convert the image data to **Unsigned char (8 bit)** and adjust as necessary with offset and scaling to produce an image with a range of **0 to 255**.

4.1.4. Isolate only the bone region in the converted image and crop around the bounds of the bone. Record the dimensions of the cropped images.

4.1.5. Save as **2D TIFF** format.

4.1.6. Open the image, change the type to **16-bit**, and save it as a single **3D TIFF** file.

4.2. Surface reconstruction

4.2.1. Generate surfaces from the segmentation labels, **smooth** and **decimate** the surfaces iteratively, ensuring that the faces are never reduced by more than half in any single iteration.

NOTE: Using the described process, the target number of faces is approximately 30,000 for each proximal and distal femur surface and 70,000 for each hemi-pelvis surface.

4.2.2. Export the surfaces as a surface mesh in *.vtk format for use as a model file for landmark identification.

4.3. Landmark identification for the coordinate system

4.3.1. Identify landmarks of the femur for generation of the femoral coordinate system (**Figure 5**).

NOTE: The parameters provided below are specific to the referenced dataset and imaging protocols; values may need to be altered to select the landmarks appropriately.

4.3.1.1. Open the **proximal femur** as a **model file**. Open the **Post** toolbar and **Data** panel to add a standard field of **1-Princ Curvature**. Over-select the **faces of the femoral head**, select a **smoothness** of **10**, and then **apply**. From the **edit** panel, **select range** to include only negative curvature. **Export** this femoral head surface as a surface mesh in *.k format for a **sphere fit** to determine the center of the femoral head.

4.3.1.2. Using a similar process, apply **1-Princ Curvature** to the **distal femur** with the **smoothness** of **5** and again **select range** to include only the faces with negative curvature. **Export** this **femoral condyle** surface for a **cylinder fit** to determine the medial-lateral axis.

4.3.1.3. Apply **2-Princ Curvature** to the distal femur, using a **smoothness** of **3**. Highlight the ridges of the epicondyles and **select range** using an upper cut-off of -0.1. **Export** these faces to generate a plane and use it to isolate the faces of the posterior condyles for the cylinder fit.

4.3.2. Identify landmarks of the pelvis for generation of the pelvic coordinate system (**Figure 5**).

NOTE: The parameters provided below are specific to the referenced dataset and imaging protocols; values may need to be altered to select the landmarks appropriately.

4.3.2.1. For each hemi-pelvis, apply **2-Princ Curvature** with a **smoothness** of **5** and **select range** to include only positive faces to isolate the lunate surface of the acetabulum. **Export** the **lunate surface** and use a **sphere fit** to determine the center of the acetabulum.

4.3.2.2. Re-apply **2-Princ Curvature** with a **smoothness** of **2** and select all faces with curvature less than -0.15 to highlight the spines of the pelvis. Choose points on the edge of these spines that best represent the **ASIS** and **PSIS** as landmarks and record them.

5. Bone motion tracking

5.1. Calibration

5.1.1. Identify **12 beads** of the cube within each of the images from the dual fluoroscopy cameras (collected in step 2.2.6). Based on the calibrated distances between each of the beads of the cube and the measurements of the location of the cube within the dual fluoroscopy system, determine the spatial orientation of each fluoroscope through minimization of the sum-of-squares projection error between the projected and known bead locations.

5.1.2. Use the **grid** images to correct for image distortion and apply the correction to all images associated with that grid image.

5.1.3. Use the **motion** file to quantify the dynamic accuracy of the system and use marker-based tracking to track it.

5.2. Markerless tracking

5.2.1. Add the location of the selected landmarks to the bone-specific **parameters** file and collect the dynamic position of these landmarks in the dual fluoroscopy system as output for all tracked frames.

5.2.2. Determine the frames that will be tracked (based on the kinematic data from motion capture, see step 6.1.2) and open the markerless tracking software with the associated bone-specific **parameters** file.

5.2.3. Select a frame within the desired range with good visualization of the bone, and manually orient the CT-based digitally reconstructed radiograph (DRR) of the bone of interest (either the proximal femur or hemi-pelvis) using the six degrees of freedom available in the software (**Figure 6**).

NOTE: As most trials begin in a position similar to standing, this initial position can likely be used as an initial starting point for all trials.

5.2.4. Once the DRR of the bone appears well-aligned in both views, save the solution by clicking the **Manual** button in the **Solutions** panel.

NOTE: Every time a solution is saved, the orientation parameters and the normalized cross-correlation coefficient are plotted for reference. The normalized cross-correlation coefficient is calculated based on all pixels with non-zero values for both the fluoroscope and bone DRRs.

5.2.5. Apply the Diagonal Hessian Search (DHS) optimization step by clicking the **DHS** button within the **Solutions** panel and review the result. If the optimized result is preferred, move onto the next frame; otherwise, make any necessary adjustments, and resave by clicking the **Manual** button within the **Solutions** panel. Repeat this step until a satisfactory solution is found.

NOTE: In the case of poor image contrast, the optimization algorithm may not always produce a satisfactory result.

5.2.6. For every fifth frame, repeat this process, using the solution for the previous frame as a starting point. Use the **DHS** optimization to automate the process.

5.2.7. To complete the first pass of tracking, use another tool that interpolates via linear projection (LP) and optimizes solutions between the tracked frames by clicking the **Range of LP + DHS** button within the **Solutions** panel. In the window, enter the set of frames to be tracked and the two frames to be used for reference.

NOTE: The two reference frames can be any frames within the identified set of frames. However, the use of the first and last frames provides bounds for the orientation of the bones within the frame range, which can be beneficial when contrast is low.

5.2.8. Review and refine each frame of the trial, using both **Manual** and **DHS**-based solutions. Use the plot of parameters to ensure that the correlation coefficient is sufficiently high and that the orientation of the bone does not have sudden jumps in any parameter.

5.2.9. To ensure accurate tracking, have another researcher review the solution for each frame and make any necessary modifications to the solutions.

5.2.10. Repeat steps 5.2.1–5.2.9 for each bone.

5.3. Visualization of motion

5.3.1. Open the femur and pelvis surfaces in the software for kinematic visualization. If necessary, convert the surfaces to meshes using the **convert to mesh** function. Select both surfaces and **export** as a surface mesh in *.k format.

5.3.2. Using the output from tracking, generate a text file with the coordinate transformations for each bone and frame.

NOTE: The order of the surfaces must match the order of the transformations.

5.3.3. For visualization of kinematics, use the **kinemat** tool and the above two files from steps 5.3.1 and 5.3.2 to animate the kinematics. Verify that the animated kinematics look reasonable and that the surfaces have appropriate distance between them using either a semi-transparent surface or the **surface distance** tool. If necessary, return to step 5.2.8.

6. Data analysis

6.1. Skin marker kinematics

6.1.1. Within the motion capture software, batch-process all files to apply the static model and label markers. Once the trial is complete, remove any unlabeled trajectories.

NOTE: Due to the obstructions of the dual fluoroscopy system, more manual gap filling than usual may be required.

6.1.2. Use the kinematic and force plate data to identify dynamic events, such as toe-off or heel-strike during gait or maximum range of motion for pivoting activities. Determine the frames of interest for tracking of dual fluoroscopy data.

6.1.3. Export all trial data for kinematic processing in *.c3d format, including both analog data (i.e., trigger and force plate data) and marker trajectories.

6.1.4. Apply the desired model template file (saved as *.mdh file format) to the static trial, then assign this model to the motion files.

NOTE: For analysis, a lower limb model with a generalized International Society of Biomechanics (ISB) head-abdomen-thorax (HAT) segment and the CODA pelvis, a pelvis segment model defined by the two ASIS and the center of the PSIS landmarks, was used.

6.2. Dual fluoroscopy kinematics

6.2.1. Isolate frames of interest, ensuring that only contiguous frames that are tracked for both the femur and pelvis are included.

6.2.2. Filter landmark positions using a **lowpass Butterworth** filter (**0.12 normalized cut-off frequency** from residual analysis and **4th order filter**).

6.2.3. Use the filtered positions of the landmarks throughout each motion trial to track the dynamic position of the femoral coordinate system (**Figure 5**).

6.2.3.1. Define the femur origin as the **sphere-fit center of the femoral head**.

6.2.3.2. Define the femur z-axis (inferior-superior axis) between the **center of the knee** and the origin, pointing superiorly.

6.2.3.3. Define the femur x-axis (medial-lateral axis) as the long axis of a **cylinder fitted to the femoral condyles**, pointing to the left. To isolate the region of the condyles to be represented with a cylinder, **fit a plane** to the epicondyle surfaces and isolate the posterior portion of the femoral condyles.

6.2.3.4. Define the femur y-axis (anterior-posterior) as the cross-product of the defined z- and x-axes, pointing posteriorly. Correct the orientation of the x-axis to create an orthogonal coordinate system.

6.2.4. Use the filtered positions of the landmarks throughout each motion trial to track the dynamic position of the pelvic coordinate system (**Figure 5**).

6.2.4.1. Define the pelvis origin as the **center of the two ASIS landmarks**.

6.2.4.2. Define the pelvis y-axis (anterior-posterior axis) between the **center of the two PSIS landmarks** and the origin, pointing anteriorly.

6.2.4.3. Define the pelvis x-axis (medial-lateral axis) between the origin and **the right-side ASIS** landmark, pointing to the right.

6.2.4.4. Define the pelvis z-axis (inferior-superior axis) as the cross-product of the defined x- and y-axes, pointing superiorly. Correct the orientation of the x-axis to create an orthogonal coordinate system.

6.2.5. Generate the rotation matrix between the coordinate systems and calculate joint kinematics per MacWilliams and colleagues' Equation 11 (**Figure 7**)[21].

6.2.6. Calculate joint translations by transforming the distance between the sphere fit centers of the femoral head and the lunate surface of the acetabulum into the pelvis coordinate system.

NOTE: This provides a single vector to represent joint translation for each image frame.

6.3. Arthrokinematics

6.3.1. Visualize the kinematics as described in step 5.3 to animate subject-specific arthrokinematics (**Figure 8**).

6.3.2. Apply the **surface distance** data field to measure distances between the femur and pelvis surfaces during each dynamic activity (**Figure 8**).

NOTE: These data also provide quantification of the relative distance between joint surfaces but require interpretation to quantify joint translation.

6.3.3. Export surface-to-surface distances using the **surface distance** tool to quantify data across all participants.

6.4. Comparison with skin marker motion capture

6.4.1. Using the cube images and trigger from each motion trial, spatially and temporally sync the dual fluoroscopy and motion capture systems.

6.4.2. Transform the landmark locations used for skin marker motion capture (i.e., ASIS, PSIS, condyles) from the markerless tracking coordinate system to the motion capture coordinate system.

6.4.3. Combine these data with the marker locations from skin marker motion capture and import for kinematic and kinetic analysis and reporting. Adjust the analysis to utilize either dual fluoroscopy or skin marker locations for each landmark and compare landmark locations and kinematics between the two systems.

REPRESENTATIVE RESULTS:

Using dual fluoroscopy as a reference standard, the accuracy of skin-marker-based estimates of the hip joint center and the effect of soft-tissue artifact on kinematic and kinetic measurements were quantified[22–24]. The superior accuracy of dual fluoroscopy was then used to identify subtle differences in pelvic and hip joint kinematics between patients with FAIS and asymptomatic control participants[25]. Dual-fluoroscopy-based arthrokinematics were analyzed to quantify hip joint coverage, the relationship between morphology and kinematics, and bone-to-bone distances during dynamic motions[26–29].

Before developing a protocol to investigate weight-bearing hip joint kinematics, the system was validated in cadaveric specimens with implanted metal beads during clinical exams in a supine position to an accuracy within 0.5 mm and 0.6°[30]. Once validated, kinematics during clinical exams were measured using dual fluoroscopy in patients with FAIS and asymptomatic control participants. The results demonstrated that patients had altered motion in both internal rotation and adduction[31].

Using weight-bearing dual fluoroscopy as a reference standard, the error in identifying the location of the hip joint center as well as the errors caused by soft-tissue artifact were then directly analyzed. Functional methods of identifying the hip joint center, i.e., the star-arc motion, were identified to be superior to predictive, landmark-based methods with errors of 11.0 and 18.1 mm, respectively[32]. Dynamic errors in the hip joint center were similar to those from standing; however, an additional 2.2 mm of spurious hip joint center movement was attributed to soft tissue artifact, with errors of more than 5 cm during dynamic movement for the greater trochanter marker[23].

In addition to the errors in identification of the hip joint center, joint angles were underestimated by greater than 20° in internal-external rotation pivots[23]. While the underestimation of kinematics is cause for concern in itself, these errors reduced the measured range of motion and calculated kinetic variables during even a low range of motion activities, such as gait[24]. However, accurate dual fluoroscopy kinematic data can be difficult to incorporate into musculoskeletal models. Specifically, model marker errors were approximately 1 cm when running inverse kinematics with dual fluoroscopy-based landmark locations. While this error is relatively small compared to the 5 cm errors due to soft tissue artifact found for skin marker motion capture data, such error is an order of magnitude larger than that of bone positions measured by dual fluoroscopy.

In addition to the quantification of errors in traditional skin marker motion capture, the accuracy and methodology behind dual fluoroscopy provide the capability to evaluate even subtle differences in kinematics between cohorts, which may otherwise be hidden by the errors of the measurement technique. While differences in hip joint kinematics were not observed between patients with cam FAIS and asymptomatic control participants, differences in pelvic kinematics that would have been difficult to detect in the presence of soft-tissue artifact were identified[25]. This assessment required direct comparison between cohorts. Moreover, the potential relationship between kinematic variation and bone morphology, such as femoral anteversion, was also investigated[27]. These findings indicated the need for consideration of both morphology and biomechanics in the diagnosis of hip pathologies and the planning of conservative or surgical treatments.

A major hurdle in the use of biomechanical data in a clinical care setting is the difference in coordinate systems used by biomechanists and clinicians. In a biomechanics lab, the landmarks used to define coordinate systems of the femur and pelvis are driven by the ability to identify and track the landmarks from the skin surface during dynamic motion. In contrast, surgical coordinate systems are defined using bony landmarks identifiable during surgery with a patient supine or prone. The direct tracking of the femur and pelvis in dual fluoroscopy allowed for the evaluation of the influence of various coordinate system definitions on kinematic output[29]. The differences between coordinate system definitions resulted in kinematic offsets greater than 5°. However, these offsets were relatively consistent during motion and could be accounted for through bony landmark identification.

The combination of subject-specific bone morphology and kinematics—arthrokinematics—provides a joint-level assessment of form and function. For patients with DDH, femoral under-coverage is thought to be the cause of degeneration, and therefore, measurements of coverage are used heavily in diagnosis and surgical planning. Unfortunately, these measurements are often limited to static images, obtained with an individual supine, and only in two dimensions. Dual fluoroscopy-derived arthrokinematics were used to directly measure the variability in femoral coverage during dynamic activities[26]. Importantly, strong correlations between coverage in standing and coverage during gait when evaluated in entirety were found. Yet, regionalized coverage varied for both anterior and posterior regions of the femoral head even during the stance phase of gait.

Extra-articular impingement is a cause of pain at the hip and surrounding region and describes abnormal contact between the femur and regions of the pelvis outside the acetabulum, including the ischium and anterior inferior iliac spine. The dynamic nature of ischiofemoral impingement was evaluated through the comparison of clinical MRI-based measurements of ischiofemoral space and those during dynamic activities[28]. Therein, decreased space was observed dynamically in comparison to the standard clinical measures; sex-based differences, which could not be attributed to kinematic differences, were also identified. These methods could also be applied to evaluate joint space dynamically, providing insight into the variability of the position of the femoral head within the acetabulum and the variability across patient cohorts (**Figure 8**).

FIGURE AND TABLE LEGENDS:

Figure 1: Overhead view of the dual fluoroscopy system positioned over the instrumented treadmill for a left hip. The system is positioned to minimize the effect of scatter and maximize the field of view. The image intensifiers are positioned approximately 100–110 cm from the source of the emitter and angled 50° from one another.

Figure 2: View from the contralateral (right) side of a participant during dynamic activities. The participant is positioned between the two image intensifiers (II) such that the field of view of the dual fluoroscopy system is centered over the left hip joint. Level and incline walking, internal and external rotation pivots, and range of motion activities are performed on a treadmill platform. Abbreviation: FHJC = functional hip joint center.

Figure 3: Overhead view of the motion capture system relative to the dual fluoroscopy system. The optical motion capture system includes 10 infrared cameras and a single video-based camera and is positioned on a frame hanging from the ceiling.

Figure 4: Anterior and posterior view of the marker set used for skin marker motion capture. There are five plates with four markers each, which are positioned on the back, thighs, and shanks of the participants; all other markers are applied directly to the skin. Calibration markers are removed for dynamic motion capture. Marker labels prefaced with an R or L indicate markers on the right or left side of the body; marker labels suffixed with S, L, R, I, A, or P indicate marker locations on a marker plate, specifically superior, left, right, inferior, anterior, or posterior, respectively. Abbreviations: *SHO = shoulder; CLAV = center of clavicles; STRN = bottom of sternum; BACK_* = markers of plate placed on the lower back; *ILC = iliac crest; *ASI = anterior superior iliac spine; *PSI = posterior superior iliac spine; GRT_TRO = greater trochanter; *THI_* = markers of the respective plates placed on the thigh; *KNE_M = medial femoral condyle (knee); *KNE_L = lateral femoral condyle (knee); *TIB_* = markers of the respective plates placed on the shank (tibia); *ANK_M = medial malleolus (ankle); *ANK_L = lateral malleolus; *5^{TH} = fifth metatarsophalangeal joint; *TOE = first metatarsophalangeal joint; *HEE = calcaneus (heel).

Figure 5: Landmarks of superior iliac spine and femur. Landmarks of bilateral anterior superior iliac spine (ASIS; magenta) and posterior superior iliac spine (PSIS; cyan) and their mid-points are used to define the coordinate system of the pelvis. The center of the femoral head (orange) and bilateral femoral condyles (green), their mid-point, and a cylinder fit of the condyles are used to define the coordinate system of the femur (shown for left femur). The third axis of each bone is determined from the cross-product of the two displayed axes.

Figure 6: Dual fluoroscopy images of a left hip. At maximum rotation of the external and internal rotation pivots (center), with the image from the anterior fluoroscope (left) and the posterior fluoroscope (right). Markerless tracking solutions for the pelvis (top) and femur (bottom) for each dual fluoroscopy image.

Figure 7: Dual fluoroscopy measured kinematics. Kinematics for 100 frames surrounding the maximum rotation (vertical dotted line) of external and internal rotation pivots for a representative participant.

Figure 8: Surface distance between a left hemi-pelvis and femur. At maximum rotation of the external and internal rotation pivot (center) with respective bone models measured with dual fluoroscopy (outer).

DISCUSSION:

Dual fluoroscopy is a powerful tool for the investigation of *in vivo* kinematics, especially for the hip, which is difficult to accurately measure using traditional optical motion capture. However, fluoroscopy equipment is specialized, wherein a unique system setup may be required when imaging other joints of the human body. For example, several modifications were made to the mounting of the image intensifiers, positioning of the system, and settings of the beam energy in the application of dual fluoroscopy to the study of ankle kinematics[32–35]. In addition to requiring considerable study preparation, dual fluoroscopy requires the acquisition of additional data, including 3D medical imaging and potentially traditional skin marker motion capture to track whole-body kinematics, as well as lengthy post-processing, including CT image segmentation and markerless tracking of the acquired images. Fortunately, fully processed data from dual fluoroscopy can be used in various applications with capabilities reaching far beyond those available with traditional motion capture.

Optical motion capture utilizes the motion of markers on the skin to estimate body segment positions, while radiation-based dual fluoroscopy allows for direct measurement of only the bone positions. While significant effort has been dedicated to quantifying soft tissue dynamics relative to bone motion[36, 37], it is inherently difficult to measure the motion patterns of the large mass of soft tissue between the outer layer of skin and the bones. However, for thinner tissues in direct contact with the bones, such as the cartilage and labrum of the hip, the combination of dual fluoroscopy and CT arthrogram imaging provides the ability to dynamically evaluate their spatial relationship. The data collected during supine clinical exams were used to show that the location of clinically observed damage to the acetabular labrum aligned with the position of contact between the femur and labrum during supine impingement exams[38]. Importantly, this analysis identified that the region of initial and greatest contact between the femur and labrum did not align with the location of the smallest distance between the bones.

Individuals with hip pathoanatomy are at risk of damage to the cartilage and labrum. However, the mechanisms responsible for chondrolabral injuries are not well understood. Conceivably, arthrokinematics data built from CT arthrogram data could be analyzed to study the mechanics of the cartilage and labrum. For example, the observed penetration between surface reconstructions representing soft tissue (e.g., labrum, cartilage) and bone could be analyzed and interpreted to approximate the strain experienced by these tissues. However, even slight errors in the tracking of kinematics or reconstruction of surfaces could result in drastic differences in estimated strains and joint loads. Thus, more advanced modeling methods, such as the FE method, may be required to comprehensively evaluate chondrolabral mechanics in the hip. Data

from dual fluoroscopy, traditional skin marker motion capture of whole-body kinematics, and the instrumented treadmill can serve as input for models that estimate muscle forces and joint reaction loads and torques. These kinetic data can then serve as loading conditions to FE models that estimate chondrolabral stresses and strains.

In addition to the specific steps involved in the protocol, the scheduling of different aspects of the study is also relevant to successful data acquisition. First, in studies using arthrogram imaging, which is inherently invasive due to the injection of contrast into the hip capsule, the arthrogram must be performed either several days before or any time after the completion of motion capture experiments to avoid any effect on patient motion patterns. Second, all calibration must be performed prior to, but just before, the arrival of the participant to ensure that the system configuration is not altered between calibration and image acquisition. Third, the participant should be instructed to perform dynamic trials in a random order to eliminate any effect of ordering on the performance of tasks.

Another major consideration for the use of dual fluoroscopy for the measurement of hip kinematics is radiation exposure. It is important to note, however, that 80% of the estimated dose equivalent of radiation in the described protocol is from the CT scan. One solution to reduce exposure is the substitution of magnetic resonance imaging (MRI) for CT imaging. While MRI can be used for surface reconstruction, the tracking of dual fluoroscopy images also relies on the projection of bone densities from the digitally reconstructed radiographs. Although MRI cannot directly measure bone density, specific sequences, such as the dual echo steady state (DESS), provide some differentiation between the denser cortical bone and the less dense cancellous bone. These images can be transformed to have a similar appearance to CT images and could potentially reduce the radiation exposure of participants in dual fluoroscopy studies.

Owing to the large amount of soft tissue surrounding the hip joint, the specific positioning of the dual fluoroscopy system must be optimized to reduce X-ray scatter. The position of the participant relative to the X-ray emitters and the angle between the image intensifiers were found to be important factors. This protocol indicates the positioning of the dual fluoroscopy system used to study hip motion in participants during weight-bearing activities. It is, however, also relevant to note that the participant cohort was limited to individuals with a BMI less than 30 kg/m^2. A similar BMI limit is recommended when capturing dual fluoroscopy images of joints surrounded by large masses of soft tissue.

The protocol described herein can be applied to various dual fluoroscopy system configurations and joints, including supine and weight-bearing hip kinematics, both treadmill and overground weight-bearing ankle kinematics, and sitting shoulder kinematics[16,17,18–25,26–35]. Owing to the minimal global motion of the hip joint during treadmill gait, an instrumented treadmill was used for the assessment of weight-bearing kinematics of the hip joint. Without a treadmill or a moving fluoroscope system, it would only be possible to capture the hip joint during activities performed in a confined field of view. However, the use of a treadmill is not appropriate for all joints. As an example, application of this protocol to the investigation of ankle kinematics during treadmill walking captured only a small portion of gait due to the inherent motion of the treadmill[32,35],

while overground gait was able to capture a larger portion of gait, spanning from prior to heel-strike to after toe-off[33,40,41].

ACKNOWLEDGEMENTS:

This research was supported by the National Institutes of Health (NIH) under grant numbers S10 RR026565, R21 AR063844, F32 AR067075, R01 R077636, R56 AR074416, R01 GM083925. The content is solely the responsibility of the authors and does not necessarily represent the official views of the NIH.

DISCLOSURES:

The authors have no conflicts of interest.

REFERENCES:

1. National Center for Health Statistics (US). Health, United States, 2016: with chartbook on long-term trends in health. Hyattsville (MD): National Center for Health Statistics (US), Report No.: 2017-1232 (2017).
2. Singh, J. A., Yu, S., Chen, L., Cleveland, J. D. Rates of total joint replacement in the United States: Future projections to 2020-2040 using the national inpatient sample. *Journal of Rheumatology*. **46** (9), 1134–1140 (2019).
3. HCUPnet: A tool for identifying, tracking, and analyzing national hospital statistics. https://hcupnet.ahrq.gov/.
4. Ganz, R., Leunig, M., Leunig-Ganz, K., Harris, W. H. The etiology of osteoarthritis of the hip: An integrated mechanical concept. *Clinical Orthopaedics and Related Research*. **466** (2), 264–272 (2008).
5. Harris, W. H. Etiology of osteoarthritis of the hip. *Clinical Orthopaedics and Related Research*. **213**, 20–33 (1986).
6. Frank, J. M. et al. Prevalence of femoroacetabular impingement imaging findings in asymptomatic volunteers: A systematic review. *Arthroscopy - Journal of Arthroscopic and Related Surgery*. **31** (6), 1199–1204 (2015).
7. Anderson, L. A. et al. The 2015 Frank Stinchfield Award: Radiographic Abnormalities Common in Senior Athletes With Well-functioning Hips but Not Associated With Osteoarthritis. *Clinical Orthopaedics and Related Research*. **474** (2), 342–352 (2016).
8. Kapron, A. L. et al. Radiographic prevalence of femoroacetabular impingement in collegiate football players: AAOS exhibit selection. *Journal of Bone and Joint Surgery - Series A*. **93** (19), e111(1–10) (2011).
9. Kapron, A. L. et al. The Prevalence of radiographic findings of structural hip deformities in female collegiate athletes. *American Journal of Sports Medicine*. **43** (6), 1324–1330 (2015).
10. Garling, E. H. et al. Soft-tissue artefact assessment during step-up using fluoroscopy and skin-mounted markers. *Journal of Biomechanics*. **40** (Suppl. 1), S18–24 (2007).
11. Fuller, J., Liu, L. J., Murphy, M. C., Mann, R. W. A comparison of lower-extremity skeletal kinematics measured using skin-and pin-mounted markers. *Human Movement Science*. **16** (2–3), 219–242 (1997).
12. Leardini, A., Chiari, A., Della Croce, U., Cappozzo, A. Human movement analysis using stereophotogrammetry Part 3. Soft tissue artifact assessment and compensation. *Gait and*

Posture. **21** (2), 212–225 (2005).
13. Peters, A., Galna, B., Sangeux, M., Morris, M., Baker, R. Quantification of soft tissue artifact in lower limb human motion analysis: A systematic review. *Gait and Posture*. **31** (1), 1–8 (2010).
14. Camomilla, V., Dumas, R., Cappozzo, A. Human movement analysis: The soft tissue artefact issue. *Journal of Biomechanics*. **62**, 1–4 (2017).
15. Miranda, D. L., Rainbow, M. J., Crisco, J. J., Fleming, B. C. Kinematic differences between optical motion capture and biplanar videoradiography during a jump-cut maneuver. *Journal of Biomechanics*. **46** (3), 567–573 (2013).
16. Lin, C. C., Lu, T. W., Lu, H. L., Kuo, M. Y., Hsu, H. C. Effects of soft tissue artifacts on differentiating kinematic differences between natural and replaced knee joints during functional activity. *Gait and Posture*. **46**, 154–160 (2016).
17. Kessler, S. E. et al. A direct comparison of biplanar videoradiography and optical motion capture for foot and ankle kinematics. *Frontiers in Bioengineering and Biotechnology*. **7** , 199 (2019).
18. Henak, C. R. et al. Computed tomography arthrography with traction in the human hip for three-dimensional reconstruction of cartilage and the acetabular labrum. *Clinical Radiology*. **69** (10), e381–e391 (2014).
19. Winter, D. A. *Biomechanics and motor control of human movement*. John Wiley and Sons Inc. (2009).
20. Camomilla, V., Cereatti, A., Vannozzi, G., Cappozzo, A. An optimized protocol for hip joint centre determination using the functional method. *Journal of Biomechanics*. **39** (6), 1096–1106 (2006).
21. MacWilliams, B. A., Davis, R. B. Addressing some misperceptions of the joint coordinate system. *Journal of Biomechanical Engineering*. **135** (5), 54506 (2013).
22. Fiorentino, N. M. et al. Accuracy of functional and predictive methods to calculate the hip joint center in young non-pathologic asymptomatic adults with dual fluoroscopy as a reference standard. *Annals of Biomedical Engineering*. **44** (7), 2168–2180 (2016).
23. Fiorentino, N. M., Atkins, P. R., Kutschke, M. J., Foreman, K. B., Anderson, A. E. In-vivo quantification of dynamic hip joint center errors and soft tissue artifact. *Gait and Posture*. **50**, 246–251 (2016).
24. Fiorentino, N. M., Atkins, P. R., Kutschke, M. J., Bo Foreman, K., Anderson, A. E. Soft tissue artifact causes underestimation of hip joint kinematics and kinetics in a rigid-body musculoskeletal model. *Journal of Biomechanics*. **108**, 109890 (2020).
25. Atkins, P. R. et al. In vivo pelvic and hip joint kinematics in patients with cam femoroacetabular impingement syndrome: a dual fluoroscopy study. *Journal of Orthopaedic Research*. **38** (4), 823–833 (2020).
26. Uemura, K., Atkins, P. R., Maas, S. A., Peters, C. L., Anderson, A. E. Three-dimensional femoral head coverage in the standing position represents that measured in vivo during gait. *Clinical Anatomy*. **31** (8), 1177–1183 (2018).
27. Uemura, K., Atkins, P. R., Fiorentino, N. M., Anderson, A. E. Hip rotation during standing and dynamic activities and the compensatory effect of femoral anteversion: An in-vivo analysis of asymptomatic young adults using three-dimensional computed tomography models and dual fluoroscopy. *Gait and Posture*. **61**, 276–281 (2018).

28. Atkins, P. R. et al. In vivo measurements of the ischiofemoral space in recreationally active participants during dynamic activities: a high-speed dual fluoroscopy study. *American Journal of Sports Medicine*. **45** (12), 2901–2910 (2017).
29. Uemura, K., Atkins, P. R., Anderson, A. E. The effect of using different coordinate systems on in-vivo hip angles can be estimated from computed tomography images. *Journal of Biomechanics*. **95**, 109318 (2019).
30. Kapron, A. L. et al. Accuracy and feasibility of dual fluoroscopy and model-based tracking to quantify in vivo hip kinematics during clinical exams. *Journal of Applied Biomechanics*. **30** (3), 461–470 (2014).
31. Kapron, A. L., Aoki, S. K., Peters, C. L., Anderson, A. E. In-vivo hip arthrokinematics during supine clinical exams: Application to the study of femoroacetabular impingement. *Journal of Biomechanics*. **48** (11), 2879–2886 (2015).
32. Roach, K. E. et al. In vivo kinematics of the tibiotalar and subtalar joints in asymptomatic subjects: a high-speed dual fluoroscopy study. *Journal of Biomechanical Engineering*. **138** (9), 0910061–0910069 (2016).
33. Roach, K. E., Foreman, K. B., Barg, A., Saltzman, C. L., Anderson, A. E. Application of high-speed dual fluoroscopy to study in vivo tibiotalar and subtalar kinematics in patients with chronic ankle instability and asymptomatic control subjects during dynamic activities. *Foot and Ankle International*. **38** (11), 1236–1248 (2017).
34. Lenz, A. L. et al. Compensatory motion of the subtalar joint following tibiotalar arthrodesis: an in vivo dual-fluoroscopy imaging study. *The Journal of Bone and Joint Surgery. American Volume*. **102** (7), 600–608 (2020).
35. Wang, B. et al. Accuracy and feasibility of high-speed dual fluoroscopy and model-based tracking to measure in vivo ankle arthrokinematics. *Gait and Posture*. **41** (4), 888–893 (2015).
36. Challis, J. H., Pain, M. T. G. Soft tissue motion influences skeletal loads during impacts. *Exercise and Sport Sciences Reviews*. **36** (2), 71–75 (2008).
37. Dumas, R., Jacquelin, E. Stiffness of a wobbling mass models analysed by a smooth orthogonal decomposition of the skin movement relative to the underlying bone. *Journal of Biomechanics*. **62**, 47–52 (2017).
38. Kapron, A. L., Aoki, S. K., Peters, C. L., Anderson, A. E. Subject-specific patterns of femur-labrum contact are complex and vary in asymptomatic hips and hips with femoroacetabular impingement. *Clinical Orthopaedics and Related Research®*. **472** (12), 3912–3922 (2014).
39. Fiorentino, N. M. et al. Soft tissue artifact causes significant errors in the calculation of joint angles and range of motion at the hip. *Gait and Posture*. **55**, 184–190 (2017).
40. Nichols, J. A., Roach, K. E., Fiorentino, N. M., Anderson, A. E. Subject-specific axes of rotation based on talar morphology do not improve predictions of tibiotalar and subtalar joint kinematics. *Annals of Biomedical Engineering*. **45** (9), 2109–2121 (2017).
41. Nichols, J. A., Roach, K. E., Fiorentino, N. M., Anderson, A. E. Predicting tibiotalar and subtalar joint angles from skin-marker data with dual-fluoroscopy as a reference standard. *Gait and Posture*. **49**, 136–143 (2016).
42. Kolz, C. W. et al. Reliable interpretation of scapular kinematics depends on coordinate system definition. *Gait and Posture*. **81**, 183–190 (2020).
43. Kolz, C. W. et al. Age-related differences in humerothoracic, scapulothoracic, and glenohumeral kinematics during elevation and rotation motions. *Journal of Biomechanics*. **117**,

110266 (2021).

Fig. 1

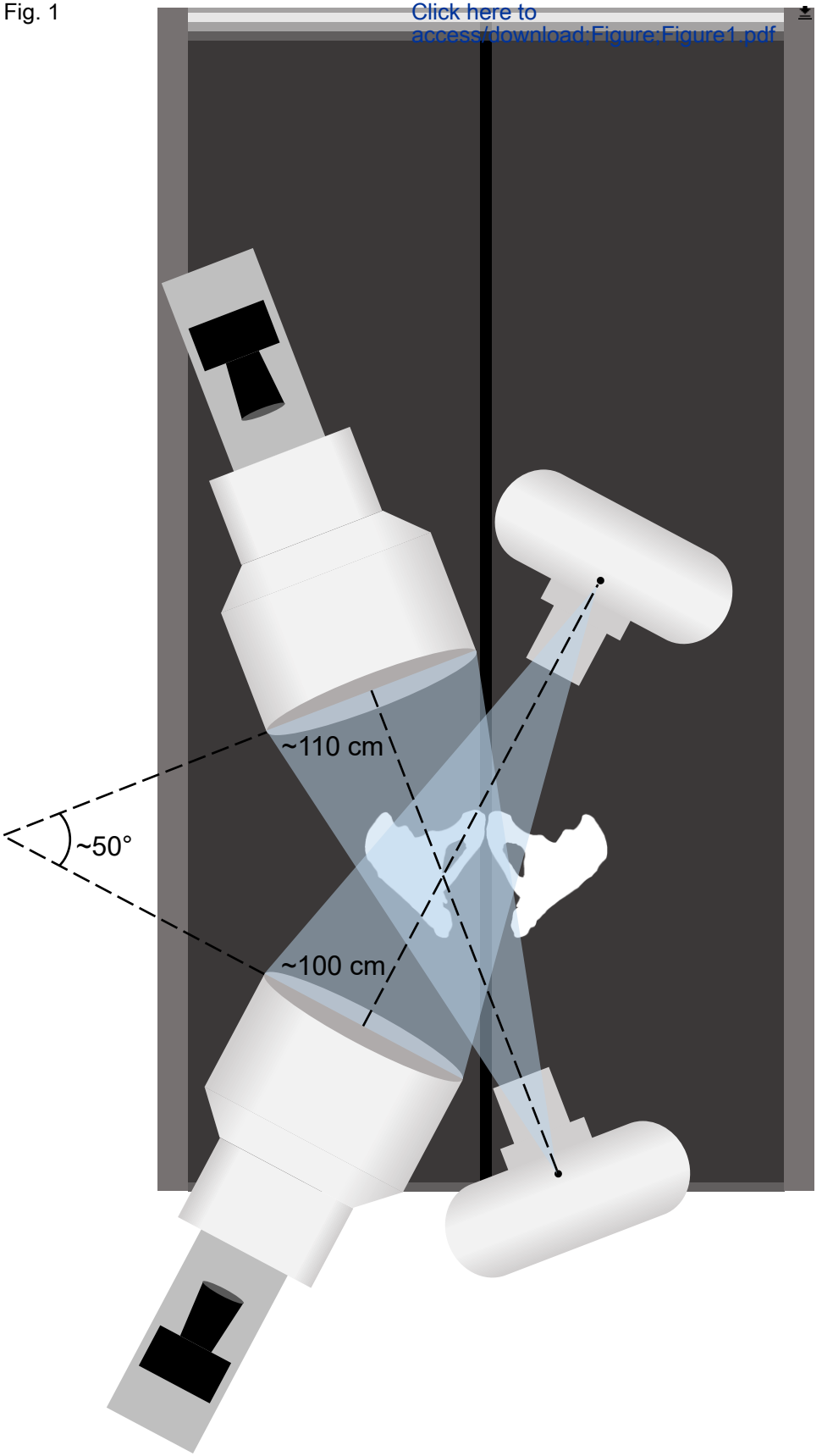

Fig. 2

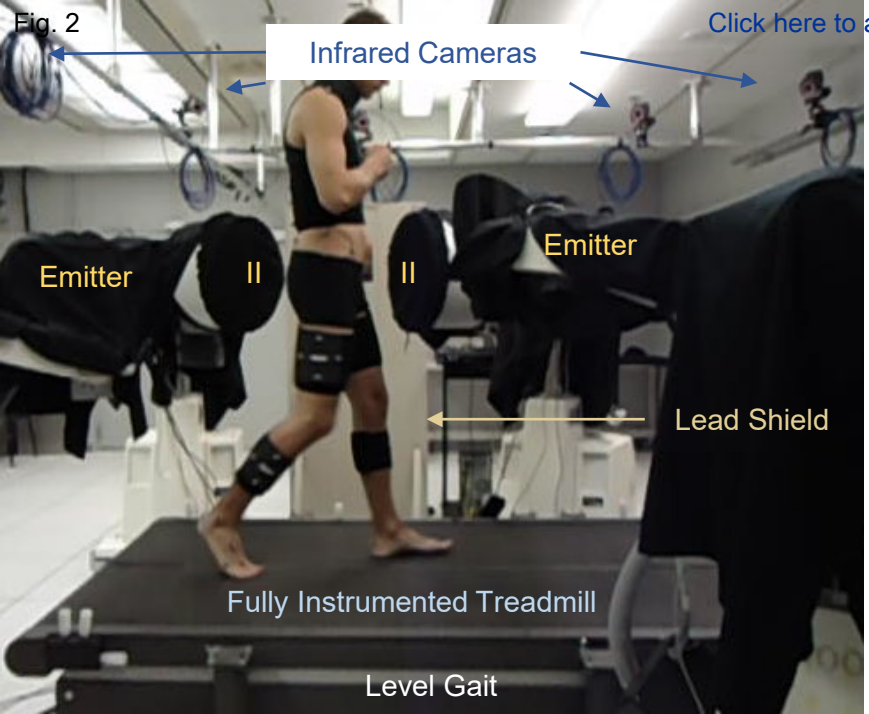

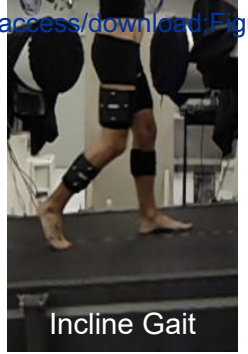

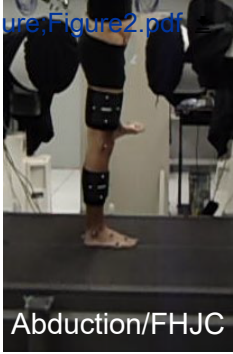

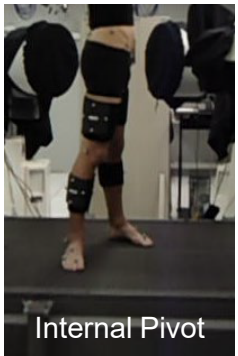

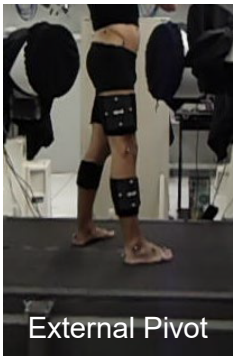

Fig. 3

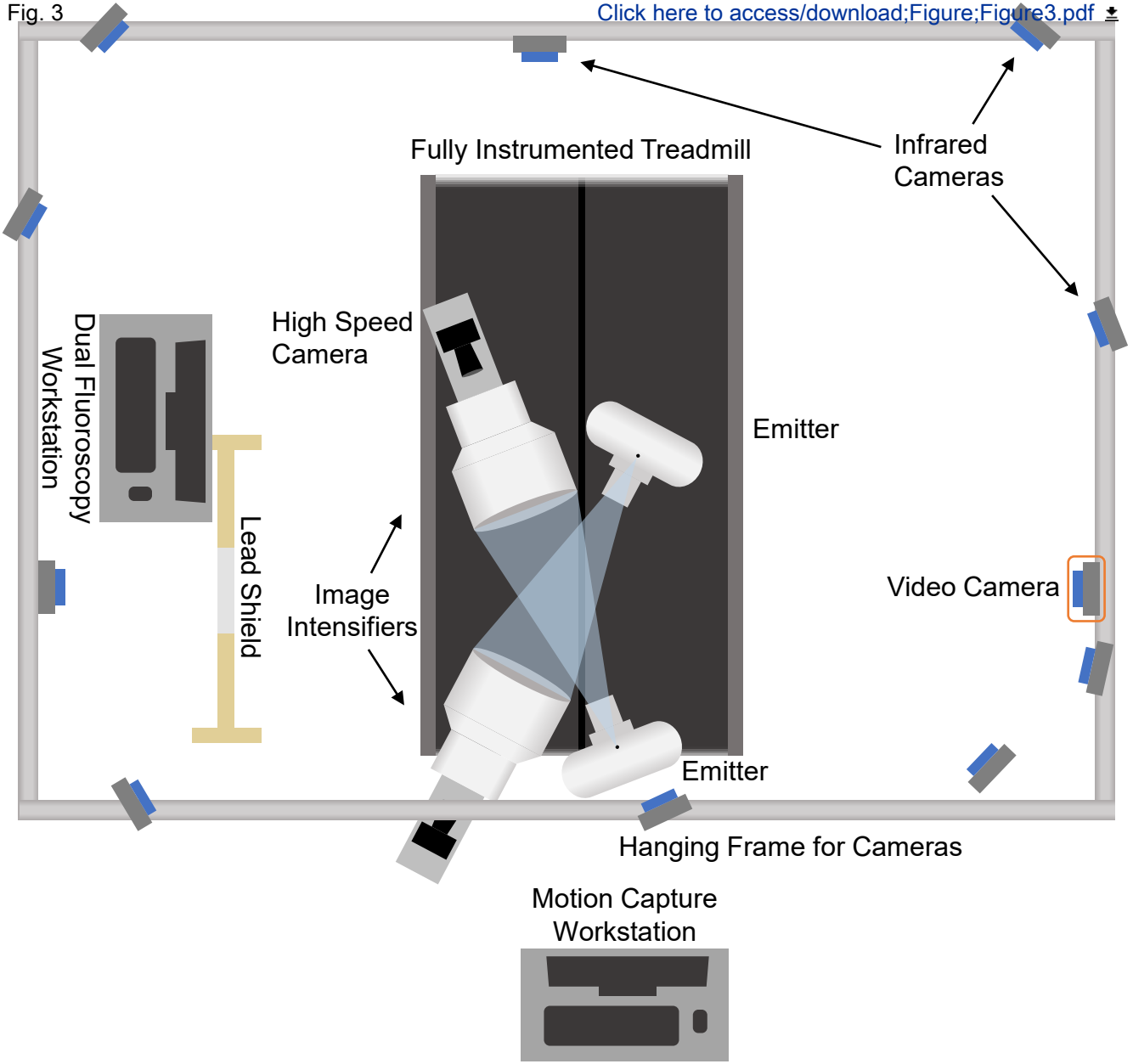

Fig. 4

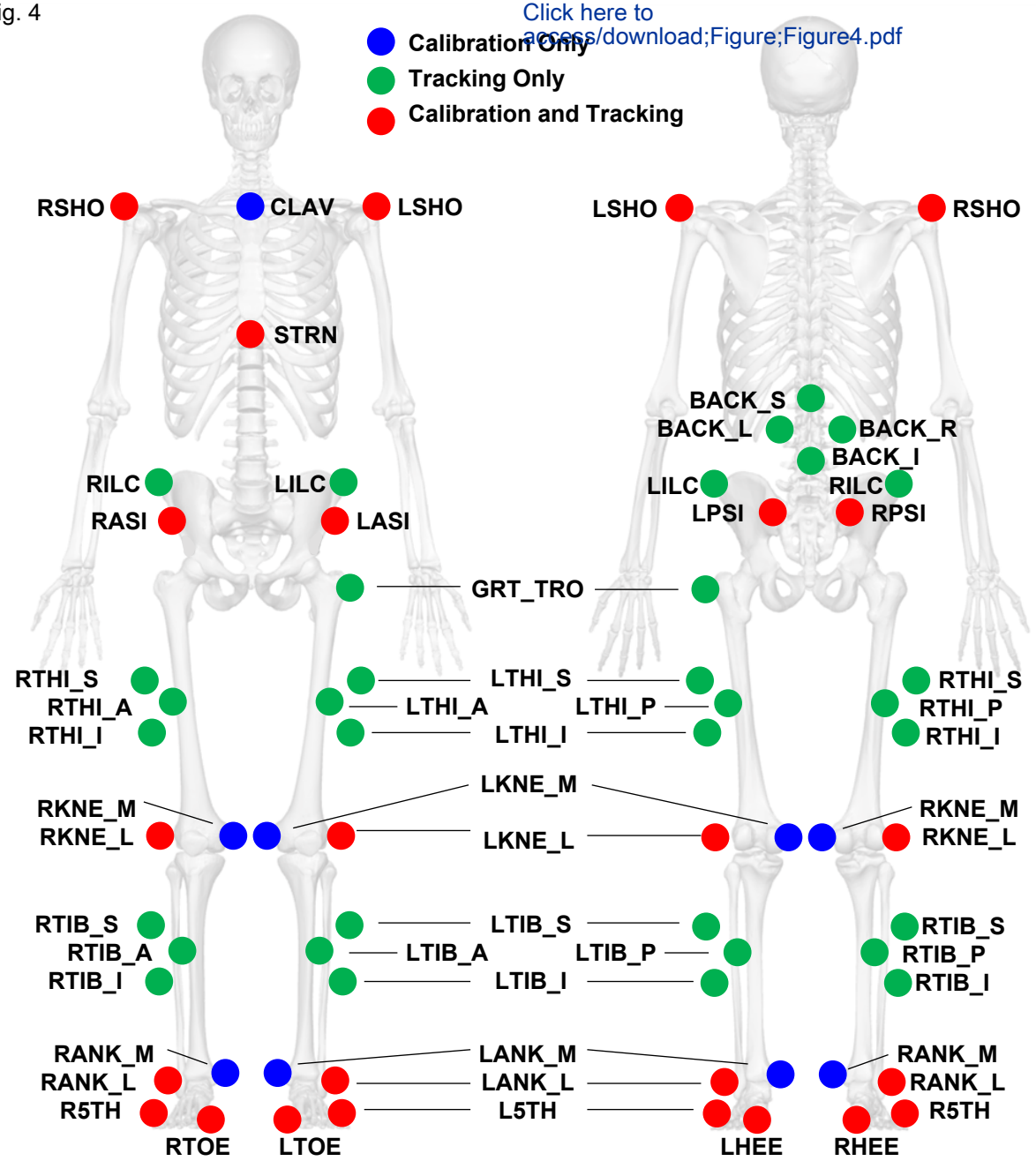

Fig. 5

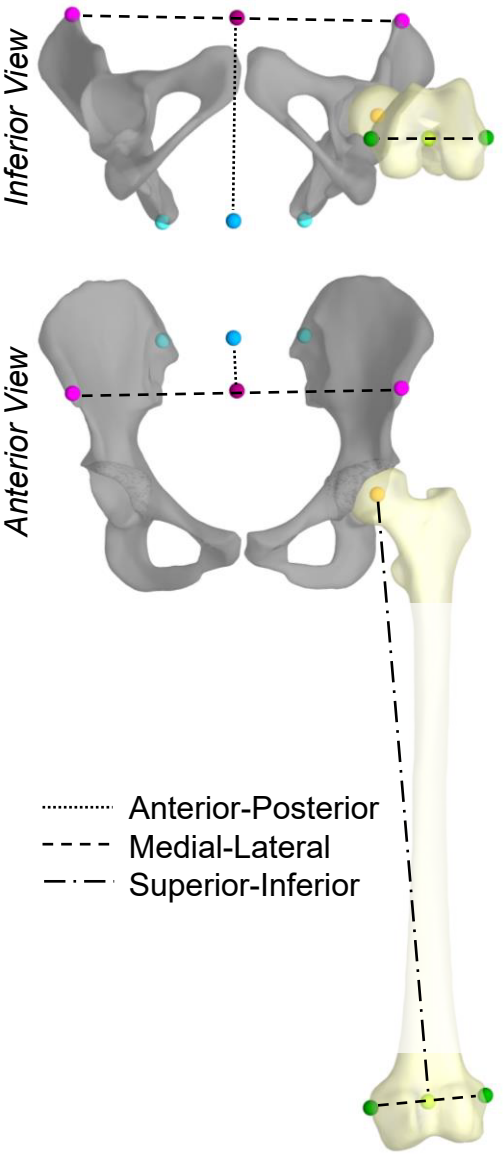

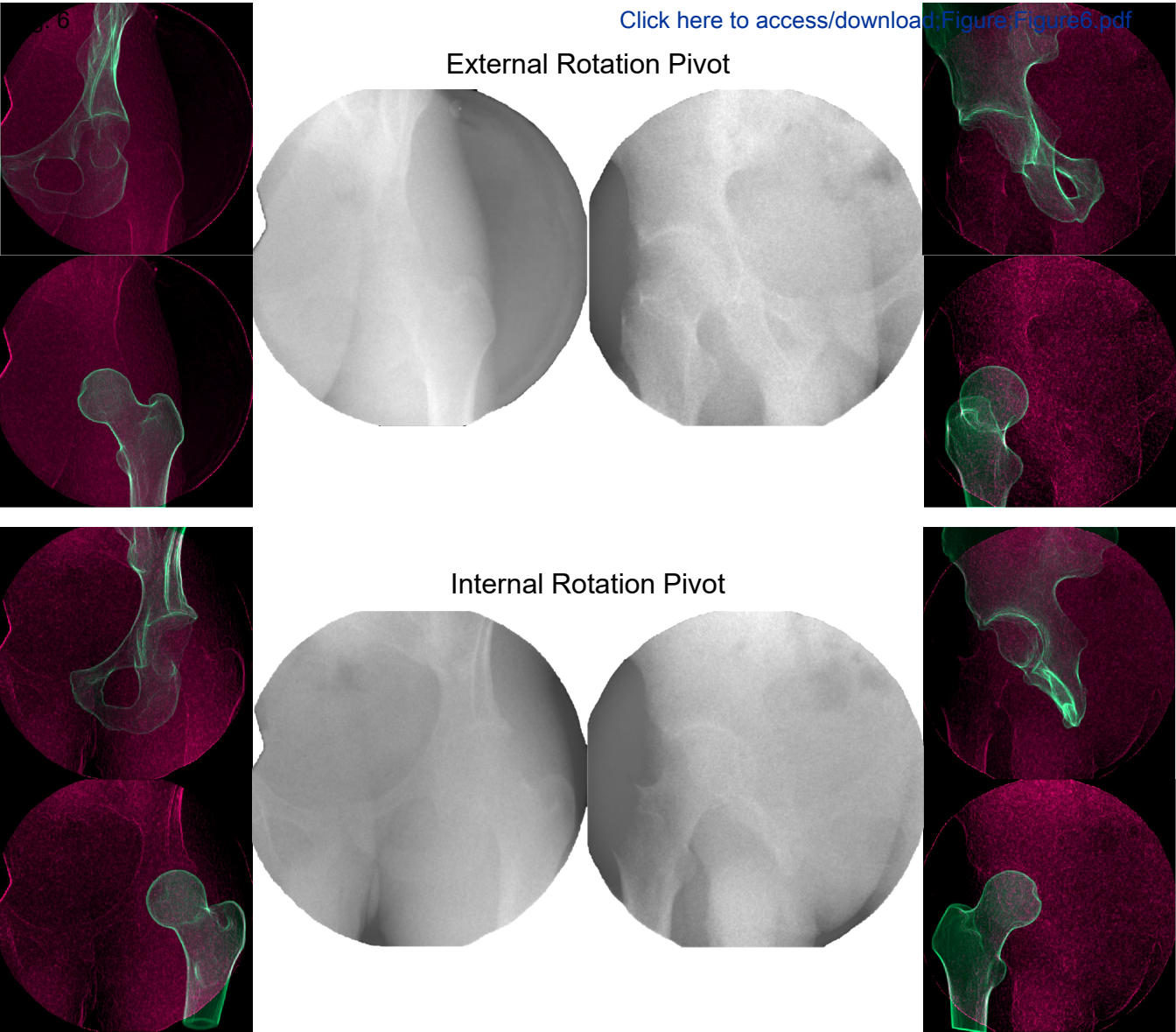

Fig. 7

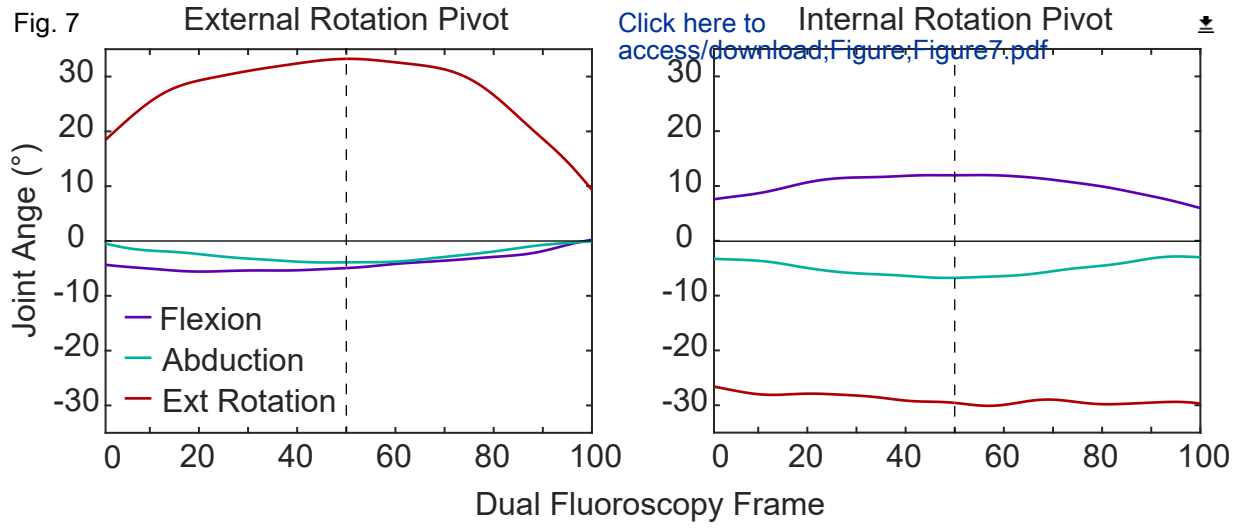

Fig. 8

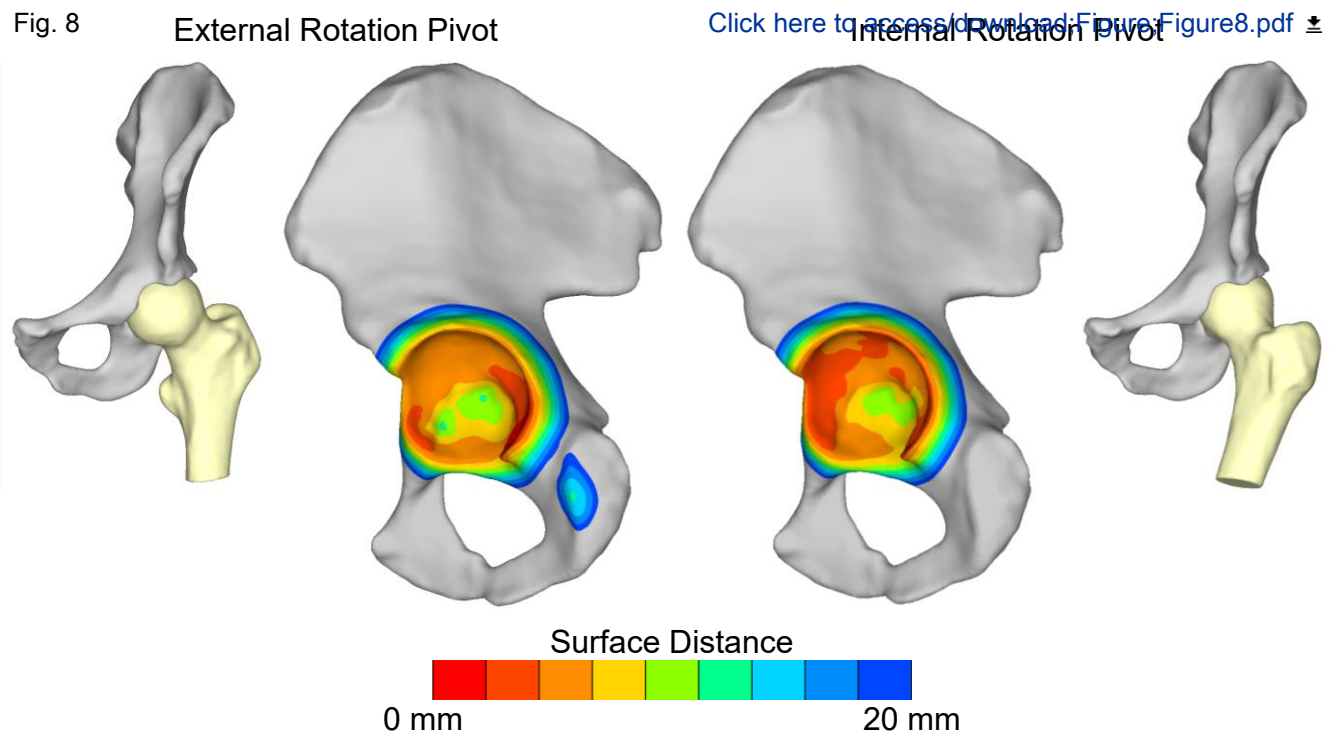

All Reviewer comments have been copied directly including any original line numbers and are shown in *italics*, while responses and revisions have been indented in plain text with line numbers referencing the edited version of the re-submission. We believe the comments of the Editors and Reviewers have made this a much stronger submission.

Editorial Comments:

1. Please take this opportunity to thoroughly proofread the manuscript to ensure that there are no spelling or grammar issues.

Response: Thank you, the authors have reviewed the manuscript for such errors and have corrected them as appropriate.

2. Please revise the text to avoid the use of any personal pronouns (e.g., "we", "you", "our" etc.).

Response: All instances of personal pronouns have been removed from the manuscript and replaced with more general and directed text.

3. JoVE cannot publish manuscripts containing commercial language. This includes trademark symbols (™), registered symbols (®), and company names before an instrument or reagent. Please remove all commercial language from your manuscript and use generic terms instead. All commercial products should be sufficiently referenced in the Table of Materials.

For example: Phantom Camera Control, FEBioStudio

Response: All software names (e.g. Phantom Camera Control, FEBioStudio, ImageJ, etc.) have been removed, as requested.

4. Please adjust the numbering of the Protocol to follow the JoVE Instructions for Authors. For example, 1 should be followed by 1.1 and then 1.1.1 and 1.1.2 if necessary. Please refrain from using bullets or dashes.

Response: The authors acknowledge their previous use of introductory paragraphs to each section and have removed these and added a summarizing paragraph of data coordination as part of the introduction instead. The protocol is now numbered entirely as described in the JoVE Instructions for Authors with each step labeled with the full step number.

5. Please include an ethics statement before the numbered protocol steps, indicating that the protocol follows the guidelines of your institution's human research ethics committee.

Response: An ethics statement was included just before the numbered protocol steps, as requested.

Revision, Lines 103-104: "Procedures outlined in this protocol were approved by the University of Utah Institutional Review Board."

6. Please ensure that all text in the protocol section is written in the imperative tense as if telling someone how to do the technique (e.g., "Do this," "Ensure that," etc.). The actions should be described in the imperative tense in complete sentences wherever possible. Avoid usage of phrases such as "could be," "should be," and "would be" throughout the Protocol. Any text that cannot be written in the imperative tense may be added as a "Note." However, notes should be concise and used sparingly. Please include all safety procedures and use of hoods, etc.

Response: Thank you for identifying this lack of clarity, the protocol section has been reviewed to ensure that all steps are written in the imperative tense.

7. Please note that your protocol will be used to generate the script for the video and must contain everything that you would like shown in the video. Please add more details to your protocol steps. Please ensure you answer the "how" question, i.e., how is the step performed? Alternatively, add references to published material specifying how to perform the protocol action. Please add more specific details (e.g., button clicks for software actions, numerical values for settings, etc) to your protocol steps. There should be enough detail in each step to supplement the actions seen in the video so that viewers can easily replicate the protocol.

Response: We have added additional detail as appropriate throughout; however, it is difficult to include information such as button clicks without mentioning specific software by name.

8. Line 98: Please specify the concentration of the anesthetic used.

Response: Thank you for identifying this lack of clarity, the concentration has been included.

Revision, Line 120: "Anesthetize the soft tissue at the injection site with 2-5 ml of 1% lidocaine."

9. Line 103: Please specify the amount of contrast agent injected.

Response: The amount of contrast agent has been specified.

Revision, Line 125: "Inject a small amount of the contrast agent (<5 ml) and…"

10. Line 109-110: Please mention how the traction is applied.

Response: The manual process of applying traction has been clarified.

Revision, Lines 127-130: "When additional resistance to the injection is observed, have a study team member manually apply traction to the hip by pulling on the participant's ankle while they resist by pulling on the headboard of the table."

11. Line 131-138/216-221: Please ensure that the Protocol section consists of numbered steps. We cannot have non-numbered paragraphs/steps/headings/subheadings.

Response: Thank you for this clarification, all non-numbered paragraphs or statements have either been incorporated into numbered protocol steps or moved to the discussion.

12. Line 155-160: The Protocol should contain only action items that direct the reader to do something. Please move the discussion about the protocol to the Discussion.

Response: Thank you for identifying this inconsistency. Any discussion about the protocol has been moved outside of the specific protocol steps.

Revision, Lines 170-188: "2.1.3 Position the x-ray emitters to be pointed towards the image intensifiers. Ensure the distance between the emitter source and face of the image intensifiers is approximately 100-110 cm. Note, the recommended distance between emitter source and face of the image intensifiers will vary based on system specification and the collimator in the x-ray emitter.

2.1.4 Connect the center of the face of the image intensifier and corresponding x-ray emitter of each fluoroscope pair using strings or measuring tapes. Verify the strings (or tapes) cross at the desired location (i.e., in the expected location of the hip joint).

2.1.5 Affix the plate with three lasers to the emitter and the mirror to the image intensifier. Turn on the lasers and refine the alignment of each emitter and image intensifier based on the reflection of the lasers back to the laser source."

13. Line 196-198: Please mention how the height is measured.

Response: Additional detail has been provided for the measurement of greater trochanter height.

Revision, Lines 232-236: “To do this, palpate the thigh to find the bony prominence of the greater trochanter and locate the most superior point, as is possible. Since the superior greater trochanter is approximately at the same height as the hip joint, measure the height from the floor to this point and compare to the height estimation used to setup the dual fluoroscopy system.”

14. Please include a one-line space between each protocol step and then highlight up to 3 pages of the Protocol (including headings and spacing) that identifies the essential steps of the protocol for the video, i.e., the steps that should be visualized to tell the most cohesive story of the Protocol. Remember that non-highlighted Protocol steps will remain in the manuscript, and therefore will still be available to the reader.

Response: Space has been added between all protocol steps using standard formatting tools. Additionally, the relevant portions of the protocol have been highlighted in yellow.

15. Figure 4: Please define the terms used in the figure in the figure description (RSHO, STRN, etc.)

Response: Thank you for identifying this oversight on our part. All acronyms associated with the marker positions are now defined in the figure legend.

Revision, Lines 685-694: “Marker labels prefaced with an R or L indicate markers on the right or left side of the body; marker labels suffixed with S, L, R, I, A, or P indicate marker locations on a marker plate, specifically superior, left, right, inferior, anterior or posterior, respectively; *SHO, shoulder; CLAV, center of clavicles; STRN, bottom of sternum; BACK_*, markers of plate placed on the lower back; *ILC, iliac crest; *ASI, anterior superior iliac spine; *PSI, posterior superior iliac spine; GRT_TRO, greater trochanter; *THI_*, markers of the respective plates placed on the thigh; *KNE_M, medial femoral condyle (knee); *KNE_L, lateral femoral condyle (knee); *TIB_*, markers of the respective plates placed on the shank (tibia); *ANK_M, medial malleolus (ankle); *ANK_L, lateral malleolus; *5TH, fifth metatarsophalangeal joint; *TOE, first metatarsophalangeal joint; *HEE, calcaneus (heel).”

16. For in-text formatting, corresponding reference numbers should appear as numbered superscripts after the appropriate statement(s) before the punctuations.

Response: The author’s apologize for this editorial error and have corrected this throughout the manuscript.

Reviewer's Comments

Reviewer: 1

Manuscript Summary:

Overall, it was a well written manuscript. I do have one main suggestion as it was a bit confusing to me to figure out how each system was integrated into the overall protocol. For example, it wasn't clear if the optical marker tracking system simply synchronized temporally or temporo-spatially with the data from the dual fluoroscopy system until the very end of the protocol, or it took a lot of back and forth for me to figure how the markerless tracking was used with the fluoroscopy camera system (these two sections were quite far apart in the protocol section of the manuscript). An outline of each methodology at the beginning of the protocol section would be helpful to familiarize the reader to how each piece will fit into the experiment before a step by step description of the protocol for each piece of information (e.g. CT scans were used to develop bone models which were fit to dual fluoroscopy system images oriented in the volume using a markerless tracking system, the cube was used as a common reference to synchronize both optical and fluoroscopy systems).

Response: The authors thank the Reviewer for their review and critique of our protocol and appreciate the complexity of the procedure. We believe this summary paragraph provides important reference for future readers to prevent confusion about the coordination of the data systems.

Revision, Lines 82-97: “Due to the desire to capture whole-body kinematics with optical marker tracking simultaneously with dual fluoroscopy images, the data collection protocol requires coordination between several sources of data. Calibration of the dual fluoroscopy system utilizes plexiglass structures implanted with metallic beads that can be directly identified and tracked as markers, while dynamic bone motion is tracked using markerless tracking which utilizes only the CT-based radiographic density of the bones to define orientation. Dynamic motion is then tracked simultaneously using dual fluoroscopy and motion capture data that is spatially and temporally synced. The systems are synced spatially during calibration through concurrent imaging of a cube with both reflective markers and implanted metal beads and generation of a common coordinate system. The systems are synced temporally for each activity or capture through the use of a split electronic trigger which sends a signal to end recording of the dual fluoroscopy cameras and interrupts a constant 5V input to the motion capture system.”

Major Concerns:

None

Minor Concerns:

Line 382: Can you provide a more detailed description to the markerless tracking process for orienting the fluoroscope images? For example, from the "Markerless Tracking" section, it was initially unclear to me what exactly the markerless tracking was being utilized for.

Response: Thank you. The authors have included a summarizing paragraph describing the different aspects of data collection and analysis, including markerless tracking, as suggested by the Reviewer. We believe that this provides improved clarity about markerless tracking and the role it has in this protocol.

Line 385: It would be clearer if the specific cameras being used for this process was identified since there are 3 in this setup: flouro, video, or mocap? Speaking of this, I don't recall if the video cameras were used for anything in particular?

Response: The authors acknlowedge the confusion associated with the various cameras used herein and have clarified the type of camera throughout the protocol. We have also provided clarification about the use of the video camera, as it is not used for any quantitative analysis described.

Revision, Lines 353-354: “Note, the video camera is not specifically used for any quantification of motion, only for visual record of the motion capture.”

Line 384: Can you reiterate during what step images of the cube were collected?

Response: Thank you for this suggestion, this information will surely help the reader follow the protocol. Some additional detail has also been added for the step.

Revision, Lines 448-455: “5.1.1 Identify 12 beads of the cube within each of the images from the dual fluoroscopy cameras (collected in Step 2.2.6). Based on the calibrated distances between each of the beads of the cube and the measurements of the location of the cube within the dual fluoroscopy system, the spatial orientation of each fluoroscope is determined through minimization of the sum-of-squares projection error between the projected and known bead locations.”

Line 399-409: Orienting the bone models was done manually and then optimized via an algorithm? Is there any objective measure for the quality of fit? Even small errors during this step could have significant results when analyzing arthrokinematics.

Response: A cross-correlation coefficient is calculated for each alignment, whether the solution was derived manually or through optimization. The coefficient is relative to the overlapping non-zero voxels of the images, but is still sensitive to image noise and contrast, so it is difficult to give an objective value which should be obtained, but we also provide additional methods to evaluate the quality of the bone alignment.

Revision, Lines 473-477: "5.2.4 Once the DRR of the bone looks to be well aligned in both views, save the solution by clicking the Manual button in the Solutions panel. Every time a solution is saved, the orientation parameters and the normalized cross-correlation coefficient are plotted for reference. The normalized cross-correlation coefficient is calculated based on all pixels with non-zero values for both the fluoroscope and bone DRRs."

Revision, Lines 495-498: "5.2.8 Review and refine each frame of the trial, using both Manual and DHS based solutions. Use the plot of parameters to ensure that the correlation coefficient is sufficiently high and that the orientation of the bone does not have sudden jumps in any parameter."

Lines 450-465: The description of the coordinate systems (e.g. left) don't mesh with the labels in Figure 5 (e.g. medial-lateral).

Response: The authors thank the Reviewer for identifying this topic of potential confusion for clarification, as it was unclear as written and shown. The text has been revised to include both sets of terminology for reference.

Revision, Lines 538-547: "6.2.3.1 Define the femur origin as the sphere-fit center of the femoral head.

6.2.3.2 Define the femur z-axis (inferior-superior axis) between the center of the knee and the origin, pointing superiorly.

6.2.3.3 Define the femur x-axis (medial-lateral axis) as the long axis of a cylinder fit to the femoral condyles, pointing to the left. To isolate the region of the condyles to be represented with a cylinder, fit a plane to the epicondyle surfaces and isolate the posterior portion of the femoral condyles.

6.2.3.4 Define the femur y-axis (anterior-posterior) as the cross-product of the defined z- and x-axes, pointing posteriorly. Correct the orientation of the x-axis to create an orthogonal coordinate system."

Revision, Lines 551-560: "6.2.4.1 Define the pelvis origin as the center of the two ASIS landmarks.

6.2.4.2 Define the pelvis y-axis (anterior-posterior axis) between the center of the two PSIS landmarks and the origin, pointing anteriorly.

6.2.4.3 Define the pelvis x-axis (medial-lateral axis) between the origin and the right ASIS landmark, pointing to the right.

6.2.4.4 Define the pelvis z-axis (inferior-superior axis) as the cross-product of the defined x- and y-axes, pointing superiorly. Correct the orientation of the x-axis to create an orthogonal coordinate system."

Line 469-471: You measure joint translation using the center of a sphere. Are the results in Figure 8 generated using the center of the sphere or the modeled surface of the femoral head?

Response: Yes, this is a relevant point that requires clarification. We found the measurement of distance between joint centers to be the most straight forward method to calculate translations, however surface-to-surface distance data also provides unique information that can be used to visualize and interpret joint translation.

Revision, Lines 563-567: “6.2.6 Calculate joint translations by transforming the distance between the sphere fit centers of the femoral head and lunate surface of the acetabulum into the pelvis coordinate system. This provides a single vector to represent joint translation for each image frame.”

Revision, Lines 571-574: “6.3.2 Apply the surface distance data field to measure distances between the femur and pelvis surfaces during each dynamic activity (Figure 8). This data provides quantification of the relative distance between joint surfaces, but requires interpretation to quantify joint translation.”

Figure 6: The dark graphic surrounding the fluoroscope images is distracting.

Response: The authors acknowledge that the darkness of the image may make it difficult to visualize the dual fluoroscopy images. While we have removed the natural black background for the fluoroscopy images, we have kept the black background of the tracking images, as this is difficult to remove to the bones leaving the boundaries of the fluoroscopy images. We hope the Reviewer will find the revised Figure 6 to be more clear.

Line 485: Can you expand a bit on "then used to correct the x-axis"? I'm assuming this is just the translation of the axis to intersect the origin?

Response: This correction is to ensure that the coordinate system of each bone is orthogonal, as this is not guaranteed with the separate definition of the first two axes. This has been clarified for the coordinate system definition of both the femur and the pelvis.

Revision, Lines 545-547: “6.2.3.4 Define the femur y-axis (anterior-posterior) as the cross-product of the defined z- and x-axes, pointing posteriorly. Correct the orientation of the x-axis to create an orthogonal coordinate system.”

Revision, Lines 558-560: “6.2.4.4. Define the pelvis z-axis (inferior-superior axis) as the cross-product of the defined x- and y-axes, pointing superiorly. Correct the orientation of the x-axis to create an orthogonal coordinate system.”

Line 507: Is Camomilla et al. 2006 the correct reference?

Response: Thank you for catching this incorrect reference. The appropriate reference is now included.

Reviewer: 2

Manuscript Summary:

This manuscript describes with full details a protocol with dual fluoroscopy coupled with optical motion capture to analyse hip kinematics. Representative results are presented which illustrate the clinical relevance of having access to the bone kinematics in pathological cases as well as the technical relevance to allow validation of kinematics and kinetics computations.

Response: The authors thank the Reviewer for their review of our protocol and appreciate the provided feedback.

Minor Concerns:

Introduction: "… subcutaneous fat and muscle, that moves relative to the underlying bone, resulting in soft-tissue artifact". References, e.g. (Camomilla et al., 2017; Leardini et al., 2005; Peters et al., 2010), may be added here.

Response: Thank you, the authors note that these relevant references were not previously included and have added them as suggested.

Introduction: "…the hip joint center is difficult to both identify and track dynamically WITH AN OPTICAL MOTION CAPTURE, …"

Response: The authors thank the Reviewer for identifying this lack of clarity and have revised the sentence based on this recommendation.

Revision, Lines 66-69: “First, the joint is relatively deep within the body, such that the location of the hip joint center is difficult to both identify and track dynamically using skin-based optical motion capture, with errors on the same order of magnitude as the radius of the femoral head[10, 11].”

Introduction: "… both single and dual fluoroscopy systems have been developed". References, e.g. (Kessler et al., 2019; Lin et al., 2016; Miranda et al., 2013), may be added here. Note that the proposed references are the ones with couple optical motion capture and with natural joints. The authors may mention they are the only ones studying the hip.

Response: Thank you for identifying another opportunity to add reference to the ongoing work in this field by other groups towards the investigation of other joint systems. We have revised as suggested and added appropriate references.

Revision, Lines 74-78: “To address the lack of accurate kinematics in combination with subject-specific bone morphology, both single and dual fluoroscopy systems have been developed for analyzing other natural joint systems[15–17]. However, this technology has only recently been applied to the native hip joint, likely due to the difficulty in acquiring high-quality images through the soft-tissue surrounding the hip.”

Introduction: "optical marker tracking simultaneously with dual fluoroscopy images, which enables us to identify positions of body segments that fall outside the combined field of view of the dual fluoroscopy system, express kinematic results, relative to gait-normalized events, AND CHARACTERIZE THE SOFT TISSUE DEFORMATION AROUND PELVIS AND FEMUR".

Response: This is an excellent point that deserves explicit attention, thank you for the suggested revision.

Revision, Lines 99-102: “This coordinated protocol enables the quantification of the position of body segments that fall outside the combined field of view of the dual fluoroscopy system, expression of kinematic results relative to gait-normalized events, and characterization of the soft tissue deformation around the femur and pelvis.”

Discussion:" Soft-tissues cannot be directly tracked…". In this paragraph, even if they have not directly worked on this, the authors could also mention the possibility to qualify soft tissue deformation (and, eventually, soft tissue stiffness (Dumas and Jacquelin, 2017)) at the level of the thigh in the perspective of analysing wobbling mass effects (Challis and Pain, 2008) during weight-bearing activities.

Response: The authors agree that this is relevant research to our discussion and have modified the discussion to include this line of research.

Revision, Lines 727-735: “Optical motion capture utilizes the motion of markers on the skin to estimate body segment positions, while radiation-based dual fluoroscopy allows for direct measurement of only the bone positions. While significant effort has been dedicated to quantifying the

dynamics of soft-tissue relative to bone motion[36, 37], it is inherently difficult to measure the motion patterns of the large mass of soft-tissue between the outer layer of skin and the bones. However, for thinner tissues in direct contact with the bones, such as the cartilage and labrum of the hip, the combination of dual fluoroscopy and CT arthrogram imaging provides the ability to dynamically evaluate their spatial relationship."

References:
Camomilla, V., Dumas, R., Cappozzo, A., 2017. Human movement analysis: The soft tissue artefact issue. Journal of Biomechanics 62, 1-4.
Challis, J.H., Pain, M.T.G., 2008. Soft Tissue Motion Influences Skeletal Loads During Impacts. Exercise and Sport Sciences Reviews 36, 71-75.
Dumas, R., Jacquelin, E., 2017. Stiffness of a wobbling mass models analysed by a smooth orthogonal decomposition of the skin movement relative to the underlying bone. Journal of Biomechanics 62, 47-52.
Kessler, S.E., Rainbow, M.J., Lichtwark, G.A., Cresswell, A.G., D'Andrea, S.E., Konow, N., Kelly, L.A., 2019. A Direct Comparison of Biplanar Videoradiography and Optical Motion Capture for Foot and Ankle Kinematics. Frontiers in Bioengineering and Biotechnology 7, 199.
Leardini, A., Chiari, L., Della Croce, U., Cappozzo, A., 2005. Human movement analysis using stereophotogrammetry. Part 3. Soft tissue artifact assessment and compensation. Gait Posture 21, 212-225.
Lin, C.-C., Lu, T.-W., Lu, H.-L., Kuo, M.-Y., Hsu, H.-C., 2016. Effects of soft tissue artifacts on differentiating kinematic differences between natural and replaced knee joints during functional activity. Gait & Posture 46, 154-160.
Miranda, D.L., Rainbow, M.J., Crisco, J.J., Fleming, B.C., 2013. Kinematic differences between optical motion capture and biplanar videoradiography during a jump-cut maneuver. Journal of Biomechanics 46, 567-573.
Peters, A., Galna, B., Sangeux, M., Morris, M., Baker, R., 2010. Quantification of soft tissue artifact in lower limb human motion analysis: A systematic review. Gait & Posture 31, 1-8.